Robotic Tracking of Coherent Structures in Flows

Matthew Michini, M. Ani Hsieh, Eric Forgoston, and Ira B. Schwartz

***Abstract*—Lagrangian coherent structures (LCSs) are separatrices that delineate dynamically distinct regions in general dynamical systems and can be viewed as the extensions of stable and unstable manifolds to general time-dependent systems. Identifying LCS in dynamical systems is useful for many applications, including oceanography and weather prediction. In this paper, we present a collaborative robotic control strategy that is designed to track stable and unstable manifolds in dynamical systems, including ocean flows. The technique does not require global information about the dynamics, and is based on local sensing, prediction, and correction. The collaborative control strategy is implemented with a team of three robots to track coherent structures and manifolds on static flows, a time-dependent model of a wind-driven double-gyre flow often seen in the ocean, experimental data that are generated by a flow tank, and actual ocean data. We present simulation results and discuss theoretical guarantees of the collaborative tracking strategy.**

***Index Terms*—Distributed robot systems, marine robotics, networked robots.**

I. Introduction

In this paper, we present a collaborative control strategy for a class of autonomous underwater vehicles (AUVs) to track coherent structures and manifolds on flows. In realistic ocean flows, these time-dependent coherent structures, or Lagrangian coherent structures (LCSs), are similar to separatrices that divide the flow into dynamically distinct regions. LCSs are extensions of stable and unstable manifolds to general time-dependent flows [1], and they carry a great deal of global information about the dynamics of the flows. For two-dimensional (2-D) flows, LCSs are analogous to ridges defined by local maximum instability, and quantified by local measures of finite-time Lyapunov exponents (FTLE) [2].

Manuscript received May 9, 2013; revised November 1, 2013; accepted December 16, 2013. This paper was recommended for publication by Associate Editor S. Carpin and Editor G. Oriolo upon evaluation of the reviewers' comments. This work was supported by the Office of Naval Research. The work of M. Michini and M. A. Hsieh was supported by ONR Contract N0001411WX20079. The work of E. Forgoston was supported by NRL Award N0017310-2-C007. The work of I. B. Schwartz was supported by ONR Contract N0001412WX20083.

M. Michini and M. A. Hsieh are with the SAS Laboratory, Department of Mechanical Engineering and Mechanics, Drexel University, Philadelphia, PA 19104 USA (e-mail: mam637@drexel.edu; mhsieh1@drexel.edu).

E. Forgoston is with the Department of Mathematical Sciences, Montclair State University, Montclair, NJ 07043 USA (e-mail: eric.forgoston@montclair.edu).

I. B. Schwartz is with the Nonlinear Systems Dynamics Section, Plasma Physics Division, U.S. Naval Research Laboratory, Washington, DC 20375 USA (e-mail: ira.schwartz@nrl.navy.mil).

This paper has supplementary downloadable material available at http://ieeexplore.ieee.org. It (compressed folder) has a size of 14.7 MB. Its uncompressed size is 15.8 MB.

Color versions of one or more of the figures in this paper are available online at http://ieeexplore.ieee.org.

Digital Object Identifier 10.1109/TRO.2013.2295655

Recently, LCSs have been shown to coincide with optimal trajectories in the ocean, which minimize the energy and the time needed to traverse from one point to another [3], [4]. Furthermore, to improve weather and climate forecasting, and to better understand contaminant transport, the use of autonomous sensors is becoming more popular for the measurement of a variety of quantities of interest in the ocean. One drawback to operating sensors in time-dependent and stochastic environments like the ocean is that the sensors will tend to escape from their monitoring region of interest. Since LCSs are inherently unstable and denote regions of the flow where more escape events may occur [5], the knowledge of LCS locations is important in maintaining sensors in specific monitoring regions.

Existing works in cooperative boundary tracking for robotic teams, which relies on one-dimensional (1-D) parameterizations, include [6], [7] and [8], [9] for static and time-dependent cases, respectively. Formation control strategies for distributed estimation of level surfaces and scalar fields in the ocean are presented in [10]–[13], and pattern formation for surveillance and monitoring by robot teams is discussed in [14]–[16].

Our study is distinguished from the existing studies in that we use cooperative robots to find coherent structures without requiring a global picture of the dynamics. Building on our existing study [17], we take inspiration from [18] and design a strategy to enable a team of robots to track the stable/unstable manifolds of general 2-D conservative flows through local sensing alone. We verify the feasibility of our method through simulations with simple 2-D flow fields, including a time-dependent double-gyre model. Furthermore, we demonstrate the validity of the proposed strategy in realistic flow fields, including flows that are generated in a laboratory setting and actual ocean flows that are obtained from the Naval Coastal Ocean Model (NCOM) database [19].

The novelty of this study lies in the use of nonlinear dynamical and chaotic system analysis techniques to derive a tracking strategy for a team of robots. The cooperative control strategy leverages the spatiotemporal sensing capabilities of a team of mobile-networked robots to track the boundaries separating the regions in phase space that exhibit distinct dynamical behaviors. The proposed boundary tracking strategy relies solely on local measurements of the velocity field. The technique is quite general, and may be applied to any conservative flow. The ability to track such structures in real time has many broader implications, including planning energy and time optimal AUV/autonomous surface vehicle (ASV) paths in the ocean, improved allocation of autonomous sensor swarms for environmental monitoring and surveillance applications [20], and predicting contaminant dispersion [21].

The paper is structured as follows. We formulate the problem and outline key assumptions in Section II. The development of the cooperative control strategy is presented in Section III and

its theoretical properties are analyzed in Section IV. Section V presents our simulation results, beginning with the tracking of static boundaries in Section V-A, time-varying boundaries given by a time-dependent model of a wind-driven double-gyre in Section V-B, experimental flow fields that are generated by our coherent structure flow tank in Section V-C, and actual ocean flows in Section V-D. Finally, we conclude with a discussion of our results and directions for future work in Sections VI and VII, respectively.

II. Problem Formulation

We consider the problem of controlling a group of N planar AUVs to collaboratively track the material lines that separate regions of flow with distinct fluid dynamics. This is similar to the problem of tracking stable (and unstable) manifolds of a general nonlinear dynamical system where the manifolds separate regions in phase space with distinct dynamical behaviors. We assume the following 2-D kinematic model for each of the AUVs:

$$\dot{x}_i = V_i \cos\theta_i + u_i \tag{1a}$$

$$\dot{y}_i = V_i \sin\theta_i + v_i \tag{1b}$$

where $\mathbf{x}_i = [x_i,\, y_i]^T$ denotes the vehicle's position in the plane, V_i and θ_i denote the control inputs which are, respectively, the vehicle's speed and heading, and $\mathbf{u}_i = [u_i,\, v_i]^T$ denotes the flow velocity that is experienced/measured by the ith vehicle. Additionally, we assume that each agent can be circumscribed by a circle of radius r, i.e., each vehicle can be equivalently described as a disk of radius r.

In this study, $\mathbf{u}_i$ is provided by a 2-D planar conservative vector field that is described by a differential equation of the form

$$\dot{\mathbf{x}} = F(\mathbf{x}). \tag{2}$$

In essence, $u_i = F_x(\mathbf{x}_i)$ and $v_i = F_y(\mathbf{x}_i)$. Let B_S and B_U denote the stable and unstable manifolds of (2), respectively. In general, B_S and B_U are the separating boundaries between regions in phase space with distinct dynamics. For 2-D flows, B_* are simply 1-D curves where $*$ denotes either stable (S) or unstable (U) boundaries. For a small region centered about a point on B_*, the system is unstable in one dimension. Finally, let $\rho(B_*)$ denote the radius of curvature of B_* and assume that the minimum of the radius of curvature $\rho_{\min}(B_*) > d_{\max}$ where $d_{\max}$ is a positive constant. This last assumption is needed to ensure that the robots do not lose track of the B_* because the boundary has too many sharp turns.

The objective is to develop a collaborative strategy to enable a team of robots to track B_* in general 2-D planar conservative flow fields through local sampling of the velocity field. In this study, the focus is on the development of a tracking strategy for B_S; however, the proposed method can be easily extended to track B_U since B_U is simply a stable manifold of (2) for $t < 0$. We outline our methodology in the following section.

III. Methodology

Our methodology is inspired by the proper interior maximum (PIM) triple procedure [18]—a numerical technique designed to find stationary trajectories in chaotic regions with no attractors. While the original procedure was developed for chaotic dynamical systems, the approach can be employed to reveal the stable set of a saddle point of a general nonlinear dynamical system. The procedure consists of iteratively finding an appropriate PIM triple on a saddle straddling line segment and propagating the triple forward in time. We briefly summarize the procedure in the following section (see [18] for further details).

A. Proper Interior Maximum Triple Procedure

Given the dynamical system described by (2), let $\mathscr{D} \in \mathbb{R}^2$ be a closed and bounded set such that $\mathscr{D}$ does not contain any attractors of (2). Given a point $\mathbf{x} \in \mathscr{D}$, the escape time of $\mathbf{x}$, denoted by $T_E(\mathbf{x})$, is the time $\mathbf{x}$ takes to leave the region $\mathscr{D}$ under the differential map (2).

Let J be a line segment that crosses the stable set B_S in $\mathscr{D}$, i.e., the endpoints of the J are on opposite sides of B_S. Let $\{\mathbf{x}_L, \mathbf{x}_C, \mathbf{x}_R\}$ denote a set of three points in J such that $\mathbf{x}_C$ denotes the interior point. Then, $\{\mathbf{x}_L, \mathbf{x}_C, \mathbf{x}_R\}$ is an *interior maximum* triple if $T_E(\mathbf{x}_C) > \max\{T_E(\mathbf{x}_L), T_E(\mathbf{x}_R)\}$. Furthermore, $\{\mathbf{x}_L, \mathbf{x}_C, \mathbf{x}_R\}$ is a PIM triple if it is an interior maximum triple and the interval $[\mathbf{x}_L, \mathbf{x}_R]$ in J is a proper subset of J.

Then, the numerical computation of any PIM triple can be obtained iteratively starting with an initial saddle straddle line segment J_0. Let $\mathbf{x}_{L_0}$ and $\mathbf{x}_{R_0}$ denote the endpoints of J_0, and apply an $\varepsilon_0 > 0$ discretizing partition of J_0 such that $\mathbf{x}_{L_0} = \mathbf{q}_0 < \mathbf{q}_1 < \cdots < \mathbf{q}_M = \mathbf{x}_{R_0}$. For every point $\mathbf{q}_i$, determine $T_E(\mathbf{q}_i)$ by propagating $\mathbf{q}_i$ forward in time using (2). Then, the PIM triple in J_0 is given by the points $\{\mathbf{q}_{k-1}, \mathbf{q}_k, \mathbf{q}_{k+1}\}$ where $\mathbf{q}_k = \arg\max_{i=1,\ldots,M} T_E(\mathbf{q}_i)$. This PIM triple can then be further refined by choosing J_1 to be the line segment containing $\{\mathbf{q}_{k-1}, \mathbf{q}_k, \mathbf{q}_{k+1}\}$ and reapplying the procedure with another $\varepsilon_1 > 0$ discretization where $\varepsilon_1 < \varepsilon_0$.

Given an initial saddle straddling line segment J_0, it has been shown that the line segment given by any subsequent PIM triple on J_0 is also a saddle straddling line segment [18]. Furthermore, if we use a PIM triple $\mathbf{x}(t) = \{\mathbf{x}_L, \mathbf{x}_C, \mathbf{x}_R\}$ as the initial conditions for the dynamical system given by (2) and propagate the system forward in time by Δt, then the line segment containing the set $\mathbf{x}(t + \Delta t)$, $J_{t+\Delta t}$, remains a saddle straddle line segment. As such, the same numerical procedure can be employed to determine an appropriate PIM triple on $J_{t+\Delta t}$. This procedure can be repeated to eventually reveal the entire stable set B_S and unstable set B_U within $\mathscr{D}$ if time was propagated forward and backward, respectively.

Using the ideas from the PIM triple procedure, our objective is to devise a cooperative control strategy for a team of N robots to track the stable (and unstable) manifolds of a general conservative time-independent flow field $F(\mathbf{x})$. Similar to the PIM triple procedure, we propose a *saddle straddle* control strategy for a team of $N \geq 3$ robots. Different from the PIM triple procedure, our robots will rely solely on information that

can be gathered via local sensing and shared throughout the network. In contrast, a strict implementation of the PIM triple procedure would require the global knowledge of the system dynamics throughout a given region, since the method relies on computing escape times. We describe our approach in the following section.

B. Controller Synthesis

Consider a team of three robots and identify them as robots $\{L, C, R\}$. While the robots may be equipped with similar sensing and actuation capabilities, we propose a heterogeneous cooperative control strategy.

Let $\mathbf{x}(0) = [\mathbf{x}_L^T(0), \mathbf{x}_C^T(0), \mathbf{x}_R^T(0)]^T$ be the initial conditions for the three robots. Assume that $\mathbf{x}(0)$ lies on the line segment J_0, where J_0 is a saddle straddle line segment and $\{\mathbf{x}_L(0), \mathbf{x}_C(0), \mathbf{x}_R(0)\}$ constitutes a PIM triple. Similar to the PIM triple procedure, the objective is to enable the robots to maintain a formation such that a valid saddle straddle line segment can be maintained between robots L and R. Different from the PIM triple procedure, rather than computing escape times for points on a saddle straddle line segment, robot C must remain close to B_S using only local measurements of the velocity field information provided by the rest of the team. As such, we refer to robot C as the tracker of the team, while robots L and R maintain a *straddle formation* across the boundary at all times. Robots L and R may be thought of as herding robots, since they control and determine the actions of the tracking robot.

1) Straddling Formation Control: The controller for the straddling robots consists of two discrete states: a passive control state U_P and an active control state U_A. The robots initialize in the passive state U_P where the objective is to follow the flow of the ambient vector field. Therefore, $V_i = 0$ for $i = L, R$. Robots execute U_P until they reach the maximum allowable separation distance d_{Max} from robot C. When $\|\mathbf{x}_i - \mathbf{x}_C\| > d_{\text{Max}}$, robot i switches to the active control state U_A where the objective is to navigate to a point $\mathbf{p}_i$ on the current *projected* saddle straddle line segment $\hat{J}_t$ such that $\|\mathbf{p}_i - \mathbf{p}_c\| = d_{\text{Min}}$ and $\mathbf{p}_C$ denotes the midpoint of $\hat{J}_t$. When robots execute U_A, $V_i = \|a_1(\mathbf{p}_i - \mathbf{x}_i) - \mathbf{u}_i\|$ and $\theta_i(t) = \alpha_i(t)$, where α_i is the angle between the desired and current heading of robot i (as shown in Fig. 1) and $a_1 \in \mathbb{R}$ is a positive gain. In summary, the straddling control strategy for robots L and R is given by

$$V_i = \begin{cases} 0 & \text{if } d_{\text{Min}} < \|\mathbf{x}_i - \mathbf{x}_C\| < d_{\text{Max}} \\ \|a_1(\mathbf{p}_i - \mathbf{x}_i) - \mathbf{u}_i\| & \text{otherwise} \end{cases} \tag{3a}$$

$$\theta_i = \begin{cases} 0 & \text{if } d_{\text{Min}} < \|\mathbf{x}_i - \mathbf{x}_C\| < d_{\text{Max}} \\ \alpha_i & \text{otherwise.} \end{cases} \tag{3b}$$

We note that while the primary control objective for robots L and R is to maintain a straddle formation across B_S, robots L and R are also constantly sampling the velocity of the local vector field and communicating these measurements and their relative positions to robot C. Robot C is then tasked with using these measurements to track the position of B_S.

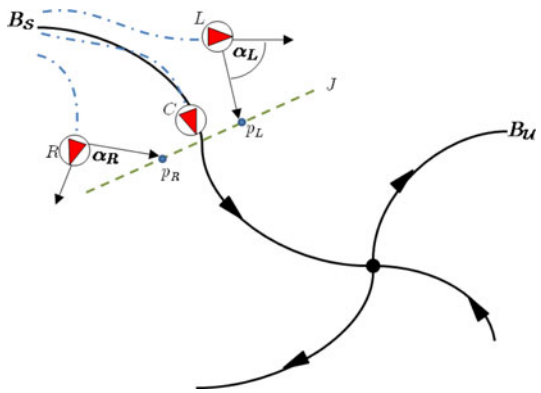

Fig. 1. Three robots tracking B_S in a given conservative vector field. The blue dash–dot lines represent the individual robot trajectories, the green-dashed line represents the saddle straddle line segment J, and $\mathbf{p}_L$ and $\mathbf{p}_R$ denote the target positions for L and R, respectively, when executing U_P and U_A.

2) Manifold Tracking Control: Let $\hat{\mathbf{u}}_L(t)$, $\hat{\mathbf{u}}_C(t)$, and $\hat{\mathbf{u}}_R(t)$ denote the current velocity measurements obtained by robots L, C, and R at their respective positions. Let $d(\cdot, \cdot)$ denote the Euclidean distance function and assume that $d(\mathbf{x}_C, B_S) < \varepsilon$ such that $\varepsilon > 0$ is small. Then, given the straddle line segment J_t such that $\mathbf{x}_L(k)$ and $\mathbf{x}_R(k)$ are the endpoints of J_t, we consider an $\varepsilon_t < \varepsilon$ discretization of J_t such that $\mathbf{x}_L = \mathbf{q}_1 < \mathbf{q}_2 < \cdots < \mathbf{q}_M = \mathbf{x}_R$. The objective is to use the velocity measurements provided by the team to interpolate the vector field at the points $\mathbf{q}_1, \ldots, \mathbf{q}_M$. Since (2) has $\mathscr{C}^1$ continuity and if $\mathbf{x}_C$ is ε-close to B_S, then the point $\mathbf{q}_B = \arg\max_{k=1,\ldots,M} \mathbf{u}(\mathbf{q}_k)^T \hat{\mathbf{u}}_C(t)$ should be δ-close to B_S where $\varepsilon < \delta < A$ and A is a small enough positive constant.

While there are numerous vector field interpolation techniques available [22]–[24], we employ the *inverse (squared) distance weighting method* described in [22] since it relies on information that can be easily obtained via a robot's onboard sensors. For a given set of velocity measurements $\hat{\mathbf{u}}_i(t)$ and corresponding position estimates $\hat{\mathbf{x}}_i(t)$, the velocity vector at some point $\mathbf{q}_k$ is given by

$$\mathbf{u}(\mathbf{q}_k) = \sum_j \sum_{i=1}^{N} \frac{w_{ij}\hat{\mathbf{u}}_i(j)}{\sum_j \sum_{i=1}^{N} w_{ij}}$$

where $w_{ij} = \|\hat{\mathbf{x}}_i(j) - \mathbf{q}_i\|^{-2}$. Rather than relying solely on the current measurements provided by the three robots, it is possible to include the recent history of $\hat{\mathbf{u}}_i(t)$ to improve the estimate of $\mathbf{u}(\mathbf{q}_k)$, i.e., $\hat{\mathbf{u}}_i(t - \Delta T)$, $\hat{\mathbf{u}}_i(t - 2\Delta T)$, and so on, where ΔT is the sampling period and $i = \{L, C, R\}$. Thus, the control strategy for the tracking robot C is given by

$$V_C = \|a_2[(\mathbf{q}_B + b\hat{\mathbf{u}}_B) - \mathbf{x}_C] - \mathbf{u}_C\| \tag{4a}$$

$$\theta_C = \beta_C \tag{4b}$$

where β_C denotes the difference in the heading of robot C and the vector $(\mathbf{q}_B - \hat{\mathbf{u}}_B)$, $a_2 \in \mathbb{R}$ is a positive gain, and b is a small number. The term $b\hat{\mathbf{u}}_B$ is included to ensure that the control strategy aims for a point in front of robot C rather than behind it. As such, the construction of the *projected* saddle straddle line segment $\hat{J}_t$ at each time step is such that $\mathbf{p}_c = \mathbf{q}_C + b\mathbf{u}_C$, $\hat{J}_t$ is

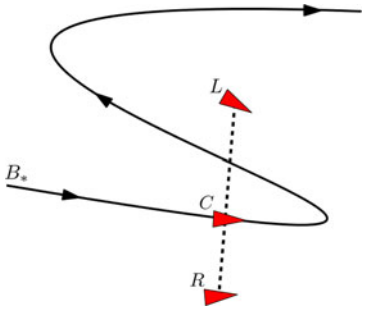

Fig. 2. Errant case illustrating the need for $d_{\mathrm{Max}} < \rho_{\mathrm{min}}(B_*)$. Here, L and R, traversing from left to right, end up on the same side of the boundary and no longer form a valid saddle straddling line segment.

orthogonal to B_S at q_C, and the length of $\hat{J}_t$ is between $2d_{\mathrm{Min}}$ and $2d_{\mathrm{Max}}$.

C. Remarks

First, it is important to note that while robots L and R execute the switching controller given by (3), the tracking robot C executes the nonswitching control strategy defined by (4). Second, since the team estimates the location of B_* by identifying the location along the saddle straddling line segment J_t, where the maximum current occurs, robots L and R must maintain the saddle straddling formation to ensure the team does not lose track of the boundary. As such, d_{Max} must be chosen such that $\rho_{\mathrm{min}}(B_*) > d_{\mathrm{Max}}$. This is to ensure that sharp turns in B_* do not cause robots L and R to end up on the same side of the boundary/manifold. Fig. 2 illustrates an errant case for which $d_{\mathrm{Max}} > \rho_{\mathrm{min}}(B_*)$. In the figure, L and R end up on the same side of the boundary and cease to maintain a saddle straddling line segment. Note that in realistic flows, $\rho_{\mathrm{min}}(B_*)$ is difficult to estimate, and, therefore, a suitable d_{Max} must be selected.

Finally, since the tracking strategy relies on identifying the region along J_t where the maximum current occurs, one way to improve the estimation of the boundary/manifold location is to increase the spatial sampling of the flow field around the neighborhood of the B_S. In this study, we achieve this by incorporating a recent history of the flow field measurements obtained by each robot but this can also be achieved by increasing the number of robots [25] or by instrumenting the robots to enable simultaneous flow measurements at different points in space. Therefore, the asynchronous nature of the formation control strategy executed by robots L and R should not impact the tracking strategy.

IV. Analysis

In this section, we discuss the theoretical feasibility of the proposed saddle straddle control strategy. We begin with the following key assumption on the robots' initial positions.

Assumption 1: Given a team of three robots $\{L, C, R\}$, assume that $d(\mathbf{x}_C(0), B_S) < \varepsilon$ for a small value of $\varepsilon > 0$, $\|\mathbf{x}_L - \mathbf{x}_C\| = \|\mathbf{x}_R - \mathbf{x}_C\| = d_{\mathrm{Min}}$ with $d_{\mathrm{Min}} > 2r$, and robots L and R are on opposite sides of B_S.

In other words, we assume that the robots initialize in a valid PIM triple formation and the positions form a saddle straddle line segment that is orthogonal to B_S. Our main result concerns the validity of the saddle straddle control strategy.

Theorem 1: Given a system of three robots with kinematics given by (1) and $\mathbf{u}_i$ given by (2), the feedback control strategies (3) and (4) maintain a valid saddle straddle line segment in the time interval $[t, t + \Delta t]$ if the initial position of the robots, $\mathbf{x}(t)$, is a valid PIM triple.

Proof: To show this, we must show that at the end of the time $t + \Delta t$, robots L and R remain on opposite sides of B_S. Consider the rate of change of the following function:

$$H(\mathbf{x}_L, \mathbf{x}_R) = \frac{1}{2}(\mathbf{x}_L - \mathbf{x}_R)^T(\mathbf{x}_L - \mathbf{x}_R).$$

This expression is simply one-half the square of the distance between robots L and R. Let J_t denote the saddle straddle line segment defined by $\mathbf{x}_L(t)$ and $\mathbf{x}_R(t)$ at t, and let $\mathbf{p}_B$ be the intersection of J_t and B_S. By construction, if we linearize (2) about the point $\mathbf{p}_B$, then the Jacobian of (2) at $\mathbf{p}_B$ will have one positive eigenvalue. Furthermore, the linearized system can be diagonalized such that the direction of instability lies along J_t [26]. Thus, $\frac{d}{dt}H > 0$ in the time interval $[t, t + \Delta t]$ when $V_i = 0$ in (3).

When $V_i \neq 0$ in (3) for $i = L, R$, $\frac{d}{dt}H < 0$ if the robots L and R are moving closer to robot C after reaching the maximum allowable separation distance. Recall $\rho_{\mathrm{min}}(B_S) > d_{\mathrm{Max}}$, the smallest radius of curvature of B_S, and $d_{\mathrm{Min}} > 2r$. Furthermore, robot C initializes ε-close to the boundary and (4) steers C toward $\mathbf{p}_C$ on the $\hat{J}_t$ where $\hat{J}_t$ is orthogonal to B_S at $\mathbf{x}_C$. This ensures that the rate of the change of the radius of curvature of the manifold B_S is small enough such that $\hat{J}_t$ intersects with B_S only once. Since $d_{\mathrm{Min}} > 2r$, this ensures that even if $\frac{d}{dt}H < 0$, the straddling robots never cross the boundary as they move closer to the tracking robot. ■

The previous theorem guarantees that for any given time interval $[t, t + \Delta t]$, the team maintains a valid PIM triple formation. As such, the iterative application of the proposed control strategy leads to the following proposition.

Proposition 1: Given a system of three robots with kinematics given by (1) and $\mathbf{u}_i$ given by (2), the feedback control strategies (3) and (4) result in an estimate of B_S, denoted as $\hat{B}_S$, such that $\langle B_S, \hat{B}_S \rangle_{L_2} < W$ for some $W > 0$, where $\langle \cdot, \cdot \rangle_{L_2}$ denotes the inner product (which provides an L_2 measure between the B_S and $\hat{B}_S$ curves).

From Theorem 1, since the team is able to maintain a valid PIM triple formation across B_S for any given time interval $[t, t + \Delta t]$, this ensures that an estimate of B_S in the given time interval also exists. Applying this reasoning in a recursive fashion, one can show that an estimate of B_S can be obtained for any arbitrary time interval. The challenge, however, lies in determining the bound on W such that $\hat{B}_S$ results in a good enough approximation since W depends on the bounds of the sensor and actuator noise, the vector interpolation routine, the sampling frequency, the time scales of the flow dynamics, and the inherent environmental noise.

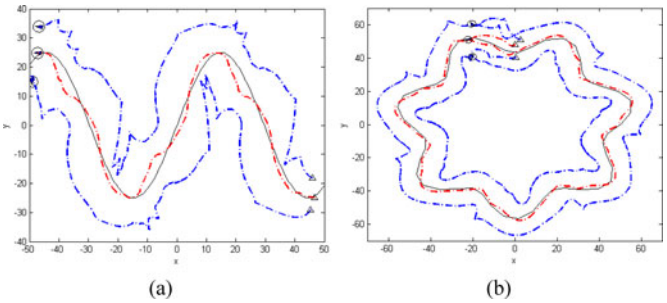

Fig. 3. Trajectories of the three-robot team tracking an (a) sinusoidal boundary and a (b) star-shaped boundary. The red-dashed line denotes the estimated position of the desired boundary shown by the solid-black line. The start positions are shown by the triangles and the end positions are shown by the circle-enclosed blue triangles.

In the following sections, we validate the proposed tracking strategy in simulations using analytical and actual flow data. In recent years, coherent structures have been observed at different length and time scales [27], [28]. Existing ocean datasets with well-known LCS boundaries are of the order of tens of kilometers that persist over multiple days to a few months [2], [3], [29]. While real ocean flows are naturally stochastic, quantifying the uncertainty in actual ocean data and its impact on the proposed tracking strategy is extremely challenging and outside the scope of this paper. Therefore, in our experimental analysis, we focus on the impact of measurement noise on the performance of the tracking strategy.

V. Simulation Results

We illustrate the proposed control strategy described by (3) and (4) with some simulation results. The strategy is validated using four distinct flow fields: 1) 2-D static conservative flows; 2) 2-D periodic flows given by a time-dependent wind-driven double-gyre model; 3) 2-D flow field generated by our multirobot coherent structure test bed; and 4) ocean current data obtained from the NCOM database [19]. The results are presented in the following sections.

A. Time-Invariant Case

We first evaluate the tracking strategy using a three-robot team tracking static boundaries in conservative flows. Fig. 3(a) shows the trajectories of three robots tracking a sinusoidal boundary, while Fig. 3(b) shows the team tracking a star-shaped boundary. We note that throughout the entire length of the simulation, the team maintains a saddle straddle formation across the boundary.

In both examples, $\mathbf{u}$ was given by

$$\mathbf{u} = -a\nabla\varphi - b\nabla \times \psi$$

where $a, b > 0$ and φ is an artificial potential function such that $\varphi(\mathbf{x}) = 0$ for all $\mathbf{x} \in B_*$ and $\varphi(\mathbf{x}) < 0$ for any $\mathbf{x} \in \mathbb{R}^2/B_*$. The vector ψ is a 3×1 vector whose entries are given by $[0,\ 0,\ \gamma(x,y)]^T$ where $\gamma(x,y)$ is the curve describing the desired boundary [16]. Finally, the estimated position of the boundary is given by the position of the tracking robot, i.e., robot C.

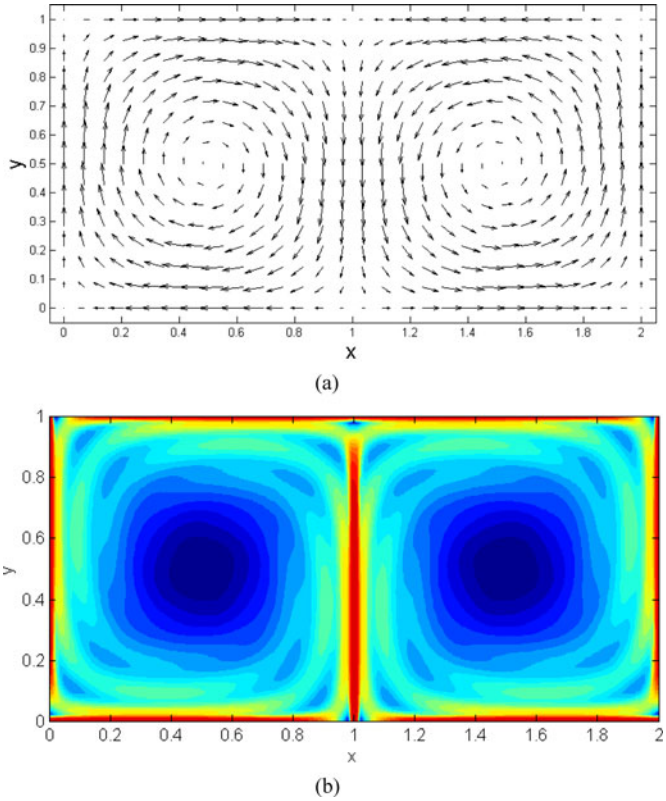

Fig. 4. (a) Phase portrait and (b) corresponding FTLE field for the model given by (5) with $A = 1$, $\mu = 0$, $\varepsilon = 0$, $\psi = 0$, and $s = 1$.

In these examples, we filtered the boundary position using a simple first-order low-pass filter.

B. Periodic Boundaries

In this section, we consider the system of three robots with kinematics given by (1), where $\mathbf{u}_i$ is determined by the wind-driven double-gyre flow model, given by

$$\dot{x} = -\pi A \sin\left(\pi \frac{f(x,t)}{s}\right) \cos\left(\pi \frac{y}{s}\right) - \mu x \tag{5a}$$

$$\dot{y} = \pi A \cos\left(\pi \frac{f(x,t)}{s}\right) \sin\left(\pi \frac{y}{s}\right) \frac{df}{dx} - \mu y \tag{5b}$$

$$f(x,t) = \varepsilon \sin(\omega t + \psi)x^2 + (1 - 2\varepsilon \sin(\omega t + \psi))x. \tag{5c}$$

When $\varepsilon = 0$, the double-gyre flow is time-independent, while for $\varepsilon \neq 0$, the gyres undergo a periodic expansion and contraction in the x-direction. In (5), A approximately determines the amplitude of the velocity vectors, $\omega/2\pi$ gives the oscillation frequency, ε determines the amplitude of the left–right motion of the separatrix between the gyres, ψ is the phase, μ determines the dissipation, and s scales the dimensions of the workspace. Fig. 4(a) shows the phase portrait of the double-gyre model for $\varepsilon = 0$, and Fig. 4(b) shows the corresponding FTLE ridges.

Fig. 5 shows the use of the control strategies (3) and (4) to track the LCS of the periodic double-gyre model. As mentioned briefly in Section I, LCSs are extensions of stable and unstable manifolds to nonautonomous dynamical systems [30]. Details

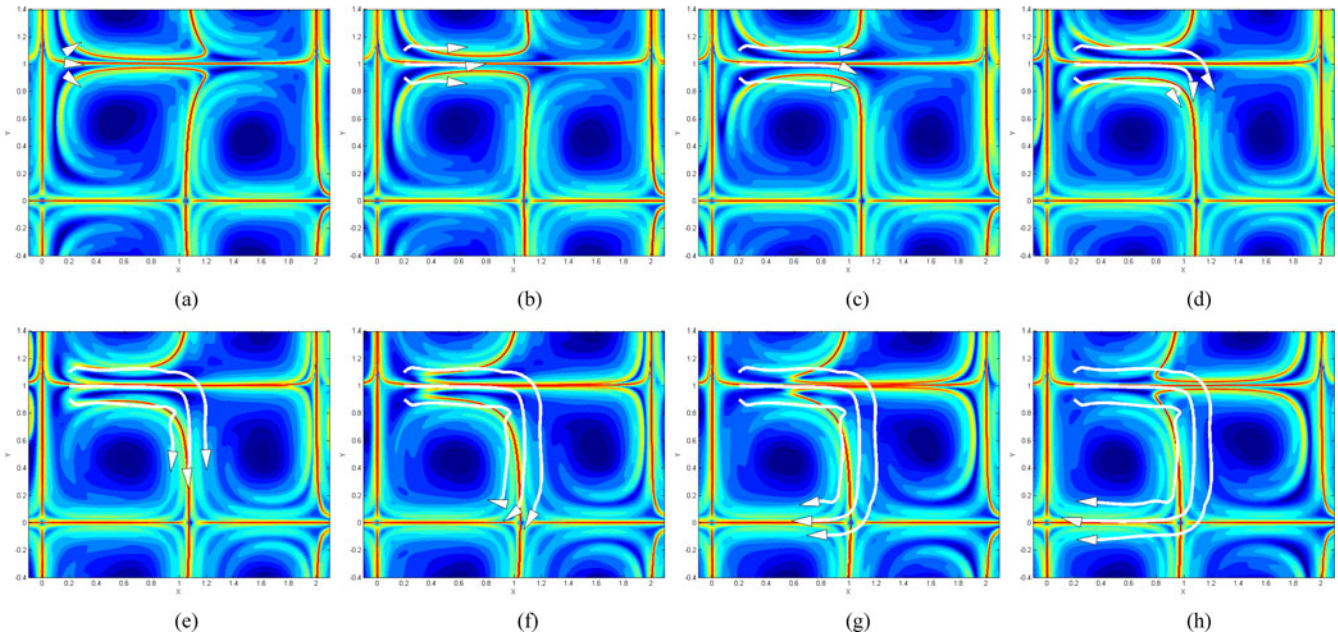

Fig. 5. Trajectories of the team of three robots tracking the LCSs of the system described by (5) with $A = 0.2$, $\mu = 0.005$, $\varepsilon = 0.1$, $\psi = 0$, $I = 0.001$, $\omega = \frac{\pi}{3}$, and $s = 1$. The FTLE integration time is $T = 4.5$. The trajectories of the robots are shown in white and the estimated LCS corresponds to the trajectory of the center robot. In this simulation, the average velocity of the team is roughly twice the mean velocity of the underlying flow field. To give a sense of time scale for the flow, most tracer particles have recirculated through the gyre after 6 s. (a) $t = 0.05$. (b) $t = 0.45$. (c) $t = 0.85$. (d) $t = 1.25$. (e) $t = 1.65$. (f) $t = 2.05$. (g) $t = 2.45$. (h) $t = 2.85$.

regarding the computation of the LCS can be found in [5] (see the supplementary multimedia file for a movie of the full simulation run). We note that while the control strategy was developed for static flows, the movie shows the robustness of the strategy for tracking LCS in time-varying flows.

To simulate the effect of measurement noise on the robustness of the control strategy, the flow velocities as measured by each robot are given by

$$u_i = \dot{x} + \eta_{x_i}(t) \tag{6a}$$

$$v_i = \dot{y} + \eta_{y_i}(t) \tag{6b}$$

for $i = \{L, C, R\}$, where $\dot{x}$ and $\dot{y}$ are given by (5) and where $\eta_{x_i}(t)$ and $\eta_{y_i}(t)$ describe stochastic white noise terms with mean zero and standard deviation $\sigma = \sqrt{2I}$, for noise intensity I. A series of simulations were performed with varying noise intensities I in (6). Fig. 6 shows the resulting tracks for different values of I. In these simulations, the remaining parameters are identical to the simulation presented in Fig. 5. In our simulations, the mean component velocity magnitude of the entire flow is 0.42, and the maximum component velocity magnitude is 0.76. We can see that the team tracks the boundaries reasonably well even with $I = 0.05$. This corresponds to a standard deviation of 0.32 for the noise, which is almost the magnitude of the mean velocity in the flow. This shows that even with significant noise, the team is still able to maintain a straddling formation across the boundary.

To further quantify the effect of noise on the tracking strategy, we simulated many tracking runs for varying values of I (with all parameters identical to the previous simulations) and recorded the number of instances (indicated by N_{fail}) for which the team failed to maintain a valid straddling formation after 1.5 s. The results are tabulated in Table I.

TABLE I
VARYING NOISE INTENSITIES AND CORRESPONDING NUMBER OF FAILURES TO MAINTAIN STRADDLING FORMATION

Noise Intensity I	N_{fail} (out of 50)	Percent Success
0.001	8	84 %
0.005	13	74 %
0.05	16	68 %
0.1	21	58 %
0.5	33	34 %

C. Experimental Flow Data

1) Background: In the results presented in the previous sections, the current measured by each vehicle is provided by the analytical models. For the results presented in this section and the following section, current velocities are provided at specific locations in the workspace. These locations are predefined and arranged in a grid within the region of interest which is set *a priori* by the measurement process. Thus, we employ a trilinear interpolation scheme in the two spatial dimensions and the time dimension to determine the current experienced/measured by each vehicle located at positions not defined on the grid. While more advanced multivariate interpolation schemes are available (e.g., tricubic), we have found that the trilinear scheme results in sufficiently smooth data for the LCS tracking and for the computation of FTLEs ridges. Indeed, it has been found that FTLE maxima are relatively insensitive to the interpolation scheme used for the computation [29].

The time-dependent double-gyre flow model given by (5) has many properties that are of interest for tracking LCS. The

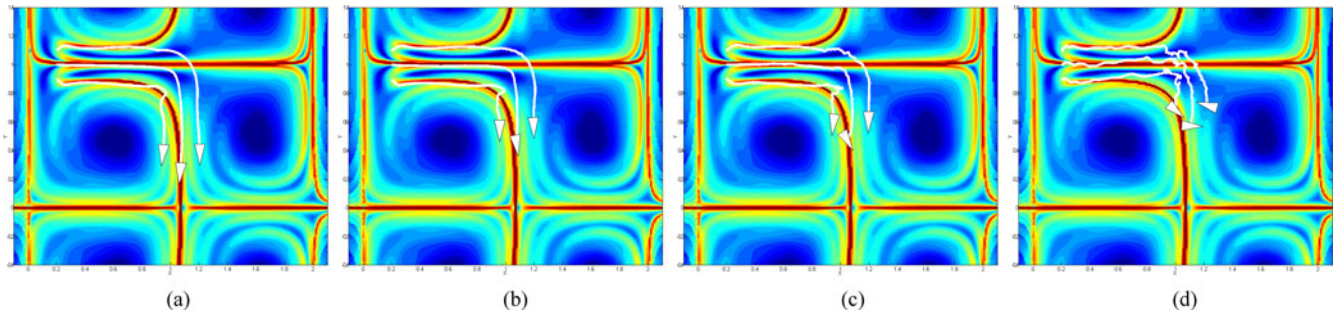

Fig. 6. Trajectories of teams of three robots performing tracking as in Fig. 5, but with increasing sensor noise intensities. In all frames, $t = 1.7$ and measurement noise is modeled as zero-mean Gaussian with $\sigma = \sqrt{2I}$. It can be seen that tracking fails with sufficiently high measurement noise. (a) $I = 0$. (b) $I = 0.005$. (c) $I = 0.05$. (d) $I = 0.5$.

model contains clear separatrices, which divide the flow into distinct regions. FTLE values for areas near the separtrices are thus high, indicating high divergence of particles starting on either side of the boundary. The FTLE field for a typical time-invariant double-gyre flow can be seen in Fig. 4(b). For 2-D flows, ridges of locally maximal FTLE values correspond, to a good approximation (see [31]), to LCS. Because of these features, we have developed an experimental test bed capable of generating controllable flow fields in a laboratory setting based on the double-gyre model.

2) Experimental Data: To create a more realistic experimental platform, we require a larger flow field in which more unsteady higher Reynolds number flows can be generated, still with some degree of control over perturbations. At Reynolds numbers in the range $\mathrm{Re} > O(10^4)$, sheared flows such as multiple gyres will exhibit strongly nonlinear response to driving and display complex, time-dependent flow patterns. Nevertheless, we must be able to control the coarse features of the flows, such as the mean sizes and locations of the gyres and their boundaries—in other words, the transport controlling features.

Toward that end, we have constructed a $60 \times 60 \times 30$ cm^3 acrylic flow tank [32]. Desired flow fields are created using 12 geared dc motors each attached to an acrylic cylinder approximately 6 cm in diameter and 12 cm in height. The motors are equipped with encoders to allow closed-loop control over the speed and direction. Each motor is thus independently controllable in order to allow the creation of complex time-varying flows. The motorized cylinders are mounted perpendicular to the bottom of the flow tank as shown in Fig. 7.

To generate the desired flow field, the tank was filled with water to a height of 14 cm. A time-invariant flow field was created by arranging the motors in a 4×3 grid and setting each motor to rotate in a sense opposite to that of its immediate neighbors. To track the flow velocity, particle image velocimetry (PIV) was employed using small paper tracer particles spread throughout the water surface. A typical output velocity field and the corresponding FTLE field are shown in Fig. 8.

Fig. 9 shows the trajectories of a three-robot team using the control strategies (3) and (4) to track the coherent structures generated in our experimental test bed. In these experiments, all the rotating cylinders were set at constant speed; as such, the coherent structures in the flow are approximately time-independent but stochastic. Quantitative analysis and comparison of the experimental flow data with the analytical gyre model show good correspondence and is described in [32]. See the supplementary video of this tracking strategy in action.

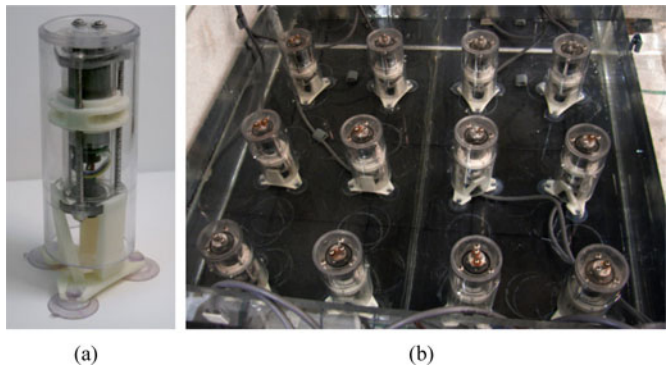

Fig. 7. Motor/cylinder unit (a) used to create controlled flows and (b) the experimental flow tank.

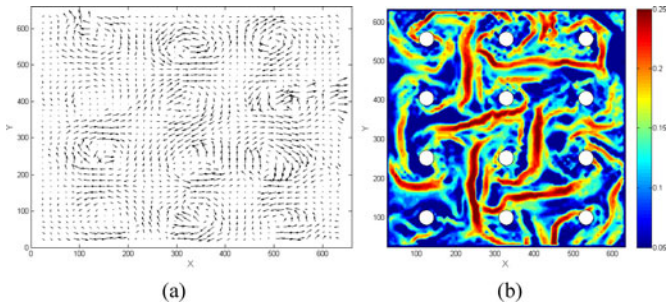

Fig. 8. (a) PIV-derived velocity field in the experimental flow tank and (b) corresponding FTLE field, with locations of the 12 rotating cylinders overlayed.

D. Ocean Flows

Finally, we implemented the control strategies (3) and (4) on a three-robot team using ocean data provided by the NCOM database hosted by the Scripps Institution of Oceanography at the University of California, San Diego, CA, USA [19].

Specifically, we considered the Santa Barbara Channel along the California coast. This area is instrumented with several high-frequency radar stations, which provide hourly surface current measurements on a 2-km grid. Fig. 10 shows a snapshot of the

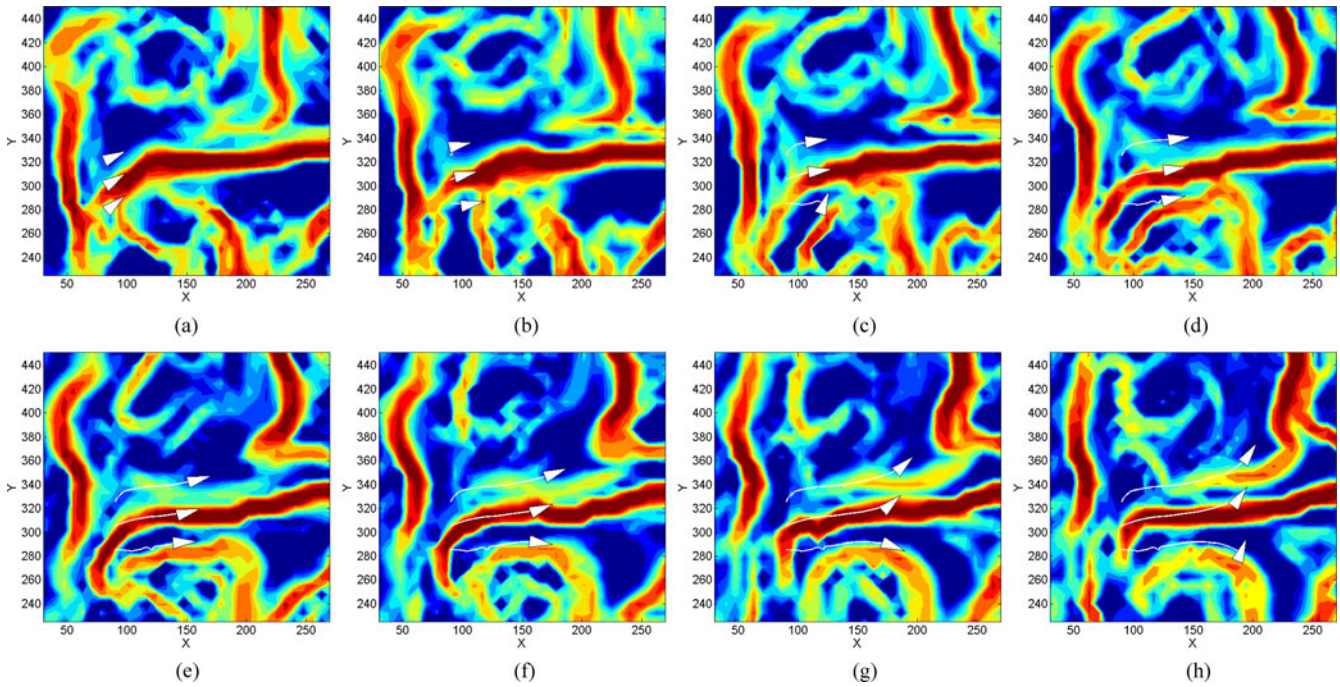

Fig. 9. Trajectories of three simulated robots tracking a coherent structure using data obtained from the experimental test bed. In this simulation, the average velocity of the robots is slightly higher than the mean velocity of the underlying flow. To give a sense of time scale, tracer particles take roughly 10 s to recirculate through the gyres. (a) $t = 0$. (b) $t = 0.8$. (c) $t = 1.6$. (d) $t = 2.4$. (e) $t = 3.2$. (f) $t = 4.0$. (g) $t = 4.8$. (h) $t = 5.6$.

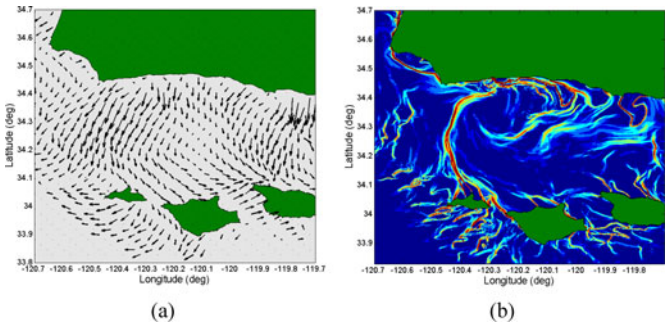

Fig. 10. (a) Surface ocean velocity data for the Santa Barbara Channel obtained via high-frequency radar measurements and (b) the corresponding FTLE field computed with an integration time of 24 h. Red hues denote high FTLE values, while blue hues denote low values.

measured velocity field and the associated FTLE field for the Santa Barbara Channel during a strong eddy event in May 2012. This area is interesting because there is a recurring small-scale eddy (roughly 40 km in diameter), which appears between the Channel Islands and the mainland. This eddy results in an area of highly divergent flow stringing between the mainland and San Miguel Island, which can be easily seen as a ridge of high FTLE values in Fig. 10(b).

We use the actual radar-derived surface velocities as the underlying vector field for a team of three simulated AUVs/ASVs to track the Santa Barbara FTLE ridge. In our simulations, we first compute the appropriate waypoints for the AUVs/ASVs team and determine the appropriate control inputs. This strategy is a slight modification to the proposed strategy and was chosen as a way to smooth out the heading commands for the robots. This slight modification also provides a more realistic strategy amenable for use with actual AUVs/ASVs.

We simulated our tracking strategy in this region over a 28-h window using data from May 16, 2012 08:00:00 GMT to May 17, 2012 12:00:00 GMT. Fig. 11 shows the team of three robots tracking a strong LCS stringing between the mainland and San Miguel Island. Even with a relatively poor initial guess of the LCS location, the team quickly forms a straddling formation and tracks the strong LCS while traversing southward. We have observed several instances where this type of persistent LCS remains across the mouth of the Santa Barbara Channel for several days. Because of its long duration, revealing LCS such as this one is useful for predicting transport phenomena at useful time scales.

VI. Discussion

In this paper, we have described a control strategy that allows collaborating robots to track coherent structures and manifolds on general static conservative flows. In addition, we showed how the strategy can be used to track LCS in time-dependent flows as well as experimental and actual ocean flows. The saddle straddle control strategy is based on the communication of local velocity field measurements obtained by each robot. Using the local velocity field information provided by the two straddling robots (the herders), one robot (the tracker) is able to detect the coherent structures, a global structure that delineates the phase space into different dynamical regions. Moreover, only initial state knowledge of the LCS is required locally to get an accurate prediction of the global structure. Our study is novel in that the robots are determining the location of a global structure based

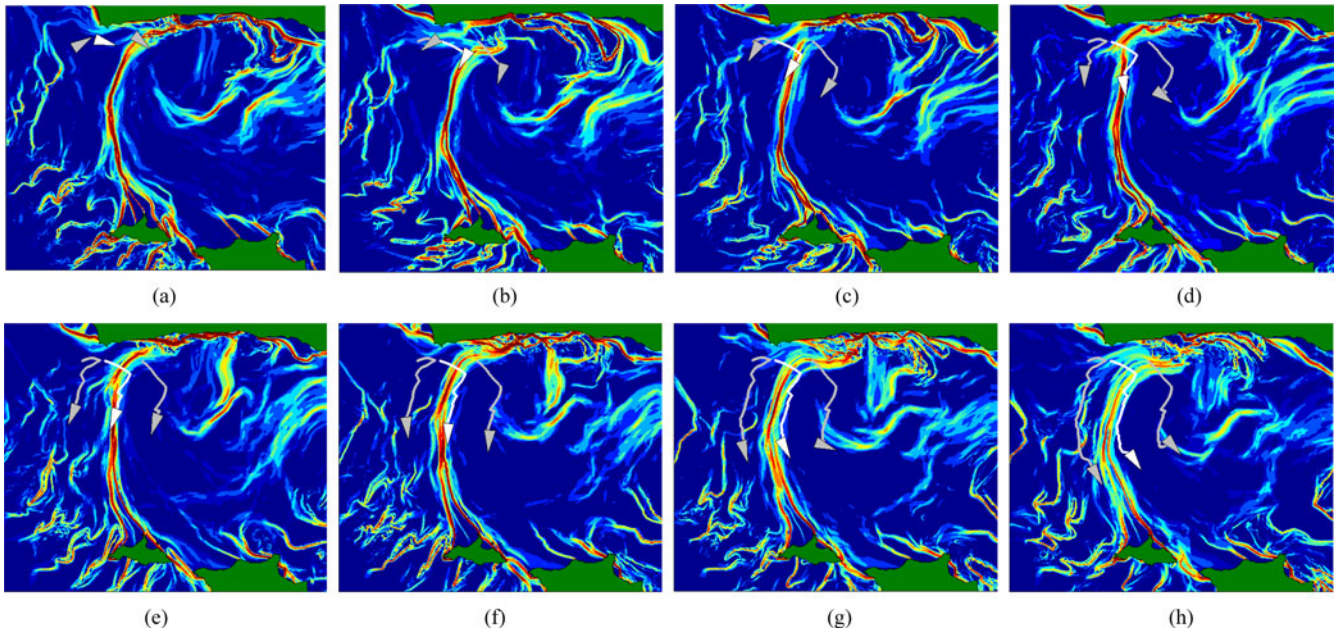

Fig. 11. Three simulated robots tracking an LCS off the coast of California over a 28-h window. The ocean surface velocities are provided by high-frequency radar measurement stations along the coast. (a) $t = 0$ h. (b) $t = 4$ h. (c) $t = 8$ h. (d) $t = 12$ h. (e) $t = 16$ h. (f) $t = 20$ h. (g) $t = 24$ h. (h) $t = 28$ h.

solely on local information, and to the best of our knowledge, tracking LCS in the ocean has never been performed using autonomous vehicles.

While the cooperative control strategy was inspired by the PIM triple procedure, a procedure that relies on the computation of escape times, which is a global property of the system, the controller itself only relies on information provided by each robot's onboard sensors. We also note that the realization of the control strategy by the team of robots can be achieved without the need for global localization information. As such, the strategy is a purely local strategy. Furthermore, the cooperative control strategy was derived to track the manifolds on a static flow, but performs surprisingly well at tracking the LCS in time-varying and stochastic flows, in the presence of large measurement noise, as well as in an actual coastal ocean situation. While this study focused on the validation of the three-robot PIM-triple-inspired tracking strategy on various flow fields, it is possible to extend this approach to larger team sizes [25]. In [25], robots L, C, and R become leaders of the team and the additional agents, or followers, take measurements of the flow and evolve under a formation control strategy prescribed by the positions of robots L, C, and R.

From our experimental test bed results, we noticed that the robots tend to veer away from the tracked LCS as they approach a local saddle/hyperbolic point in the flow. This is likely because as the team approaches the saddle point from one side, the flow reverses direction on the other side of the saddle point. As such, the robots are temporarily "pushed away" from the hyperbolic point. This can be seen from Fig. 8(b) where hyperbolic/saddle points are located in the middle of every set of four rotating cylinders. Similarly, our results using actual ocean flows show the robots veering away from the weakening and expanding LCS curve as they move southward. This seems to indicate that the tracking strategy in its present form may only be most suitable for prominent structures that are well defined and persistent. Indeed, tracking prominent structures may be more useful than weaker more transient LCSs that have a less direct impact on transport in the time scales of interest for most robotic applications.

Finally, the tracking strategy was formulated in the context of conservative flows. Since experimental and natural flows are typically nonconservative, our experimental and ocean tracking results (see Figs 9 and 11) show the robot team having difficulty maintaining a straddling formation toward the end of their tracks. This could be a consequence of the fact that these flows are not conservative, and thus the saddle straddling formation cannot be guaranteed for all times. Further inquiry is needed to better understand the impact of nonconservative flows on the tracking strategy.

VII. Future Work

In recent years, there has been significant interest in the deployment of AUVs to collect scientific data in the ocean that can impact our ability to predict harmful algal blooms, contaminant transport, and forecast weather and climate patterns. One drawback to operating sensors in time-dependent and stochastic environments like the ocean is that the sensors will tend to escape from their monitoring region of interest. As such, the ability to identify and track LCSs in these dynamic environments is highly useful to maintain appropriate sensor coverage in specific regions of interest. Additionally, since LCSs have been shown to coincide with optimal trajectories in the ocean, which minimize the energy and the time needed to traverse from one point to another [3], [4], real-time knowledge of these "superhighways" is key in planning efficient paths for AUVs. While ocean

current data can be obtained from a variety of sources, e.g., satellite sensing, ocean drifters, and high-frequency radar sensing, the data are often of low-spatiotemporal resolution and may suffer from coverage loss due to weather conditions, maintenance, etc. In addition, the long FTLE integration times required to reveal important structures in these data can cause numerical issues [29]. As such, it is of great interest to be able to locate and track LCS in areas of the ocean where sufficient velocity data coverage does not exist.

Our results show that the proposed tracking strategy can successfully track LCS present in a variety of flow fields. These attempts seem to suggest that our methods may be general enough to be applied to more complicated flow models, including multilayer PDE ocean models. As mentioned in Section IV, the robustness of the control strategy is dependent on numerous parameters in the system, which includes the robots' sensing and communication ranges, the bounds on the sensor and actuation noise, the vector interpolation technique, the sampling frequency, and the relative time scales of the AUV dynamics in relation to the surrounding flow dynamics. We believe a better understanding of the sensitivity of the proposed strategy to these various parameters will be instrumental in extending our approach to more realistic ocean conditions.

A major challenge in LCS tracking using the strategy presented is surmising the initial location of the LCS curve. This initial formation may be difficult to achieve with no prior global knowledge of the flows. By considering a team of both stationary and mobile sensors, one can potentially obtain an initial estimate of a local LCS through the stationary sensing network, which can then be tracked and further refined by the mobile nodes. Of particular interest is how we can extend our method to a swarm of heterogeneous mobile and stationary sensors (see for example [33]). Another direction for future work is to investigate how the proposed strategy scales to larger team sizes and how communication delays impact the overall accuracy of the tracking methodology. Additionally, we are also interested in determining how one can strategically place a combination of mobile and stationary sensors to provide real-time updates on the locations of LCS [20]. We believe the ability to track and potentially predict key LCS positions can lead to significant advances in the field of optimal path planning for autonomous vehicles operating in the ocean.

Finally, while the tracking strategy was formulated in the context of conservative flows, we have found that the strategy works surprisingly well in nonconservative flows. Further investigation is needed to better understand how we can achieve similar performance with provably correct guarantees in general nonconservative flows. In conclusion, while there are existing strategies to use networks of robots and sensors to track interesting phenomena in the coastal ocean [34], our strategy emphasizes the use of very limited local information about the flow to predict important global features. It is our hope that this reliance on very limited information will enable the development of more general techniques that can be implemented on realistic AUVs/ASVs for future field deployments.

REFERENCES

[1] G. Haller and G. Yuan, "Lagrangian coherent structures and mixing in two-dimensional turbulence," *Physica D*, vol. 147, pp. 352–370, Dec 2000.

[2] S. C. Shadden, F. Lekien, and J. E. Marsden, "Definition and properties of Lagrangian coherent structures from finite-time Lyapunov exponents in two-dimensional aperiodicflows," *Physica D: Nonlinear Phenomena*, vol. 212, no. 3–4, pp. 271–304, 2005.

[3] T. Inanc, S. Shadden, and J. Marsden, "Optimal trajectory generation in ocean flows," in *Proc. Amer. Control Conf.*, Jun. 8–10, 2005, pp. 674–679.

[4] C. Senatore and S. Ross, "Fuel-efficient navigation in complex flows," in *Proc. Amer. Control Conf.*, Jun. 2008, pp. 1244–1248.

[5] E. Forgoston, L. Billings, P. Yecko, and I. B. Schwartz, "Set-based corral control in stochastic dynamical systems: Making almost invariant sets more invariant," *Chaos*, vol. 21, 013116, 2011.

[6] C. Hsieh, Z. Jin, D. Marthaler, B. Nguyen, D. Tung, A. Bertozzi, and R. Murray, "Experimental validation of an algorithm for cooperative boundary tracking," in *Proc. Amer. Control Conf.*, 2005, pp. 1078–1083.

[7] S. Susca, S. Martinez, and F. Bullo, "Monitoring environmental boundaries with a robotic sensor network," *IEEE Trans. Control Syst. Technol.*, vol. 16, no. 2, pp. 288–296, Mar. 2008.

[8] I. Triandaf and I. B. Schwartz, "A collective motion algorithm for tracking time-dependent boundaries," *Math. Comput. Simul.*, vol. 70, pp. 187–202, 2005.

[9] V. M. Goncalves, L. C. A. Pimenta, C. A. Maia, B. Dutra, and G. A. S. Pereira, "Vector fields for robot navigation along time-varying curves in n-dimensions," *IEEE Trans. Robot.*, vol. 26, no. 4, pp. 647–659, Aug. 2010.

[10] F. Zhang, D. M. Fratantoni, D. Paley, J. Lund, and N. E. Leonard, "Control of coordinated patterns for ocean sampling," *Int. J. Control*, vol. 80, no. 7, pp. 1186–1199, 2007.

[11] K. M. Lynch, P. Schwartz, I. B. Yang, and R. A. Freeman, "Decentralized environmental modeling by mobile sensor networks," *IEEE Trans. Robot.*, vol. 24, no. 3, pp. 710–724, Jun. 2008.

[12] W. Wu and F. Zhang, "Cooperative exploration of level surfaces of three dimensional scalar fields," *Automatica*, vol. 47, no. 9, pp. 2044–2051, 2011.

[13] B. Reed and F. Hover, "Tracking ocean fronts with multiple vehicles and mixed communication losses," presented at the IEEE/RSJ Int. Conf. Intell. Robots Syst., Tokyo, Japan, Nov. 2013.

[14] J. Spletzer and R. Fierro, "Optimal positioning strategies for shape changes in robot teams," in *Proc. IEEE Int. Conf. Robot. Autom.*, Barcelona, Spain, Apr. 2005, pp. 754–759.

[15] S. Kalantar and U. Zimmer. (2007). Distributed shape control of homogeneous swarms of autonomous underwater vehicles. *Auton. Robots* [Online]. *22*, pp. 37–53. Available: http://dx.doi.org/10.1007/s10514-006-9002-y

[16] M. Hsieh, S. Loizou, and V. Kumar, "Stabilization of multiple robots on stable orbits via local sensing," in *Proc. IEEE Int. Conf. Robot. Autom.*, 2007, pp. 2312–2317.

[17] M. Hsieh, E. Forgoston, T. Mather, and I. Schwartz, "Robotic manifold tracking of coherent structures in flows," in *Proc. IEEE Int. Conf. Robot. Autom.*, May 2012, pp. 4242–4247.

[18] H. E. Nusse and J. A. Yorke, "A procedure for finding numerical trajectories on chaotic saddles," *Physica D: Nonlinear Phenomena*, vol. 36, pp. 137–156, Jun. 1989.

[19] Naitonal HF RADAR network—Surface currents. (2013). [Online]. Available: http://cordc.ucsd.edu/projects/mapping/maps/

[20] K. Mallory, M. A. Hsieh, E. Forgoston, and I. B. Schwartz, "Distributed allocation of mobile sensing swarms in gyre flows," *Nonlinear Process. Geophys.*, vol. 20, no. 5, pp. 657–668, 2013.

[21] T. Peacock and G. Haller, "Lagrangian coherent structures: The hidden skeleton of fluid flows," *Phys. Today*, vol. 66, no. 2, pp. 41–47, 2013.

[22] J. C. Agui and J. Jimenez. (1987). On the performance of particle tracking. *J. Fluid Mech.* [Online]. *185*, pp. 447–468. Available: http://dx.doi.org/10.1017/S0022112087003252

[23] C. Marchioli, V. Armenio, and A. Soldati, "Simple and accurate scheme for fluid velocity interpolation for Eulerian–Lagrangian computation of dispersed flows in 3D curvilinear grids," *Comput. Fluids*, vol. 36, pp. 1187–1198, 2007.

[24] E. J. Fuselier and G. B. Wright, "Stability and error estimates for vector field interpolation and decomposition on the sphere with RBFs," *SIAM J. Numer. Anal.*, vol. 47, pp. 3213–3239, 2009.

[25] M. Michini, H. Rastgoftar, M. A. Hsieh, and S. Jayasuriya, "Distributed formation control for collaborative tracking of manifolds in flows," in *Proc. IEEE Amer. Control Conf.*, Jun. 2014, to be published.
[26] P. Hartman, *Ordinary Differential Equations*, 2nd ed. Philadelphia, PA, USA: Soc. Ind. Appl. Math, 2002.
[27] K. Katija, W. Beaulieu, C. Regula, S. Colin, J. Costello, and J. Dabiri, "Quantification of flows generated by the hydromedusa aequorea victoria: A Lagrangian coherent structure (LCS) analysis," *Marine Ecol. Progr. Series*, vol. 435, pp. 111–123, Aug. 2011.
[28] G. Haller and F. Beron-Vera, "Coherent Lagrangian vortices: The black holes of turbulence," *J. Fluid Mech*, vol. 731, R4, Sep. 2013.
[29] C. S. Harrison and G. A. Glatzmaier, "Lagrangian coherent structures in the California Current System—Sensitivities and limitations," *Geophys. Astrophys. Fluid Dyn.*, vol. 106, pp. 22–44, Oct. 2010.
[30] S. Kent, "Lagrangian coherent structures: Generalizing stable and unstable manifolds to non-autonomous dynamical systems," Tech. Rep., Univ. Arizona, Tucson, AZ, USA, 2008.
[31] G. Haller, "A variational theory of hyperbolic Lagrangian coherent structures," *Physica D*, vol. 240, pp. 574–598, 2011.
[32] M. Michini, K. Mallory, D. Larkin, M. A. Hsieh, E. Forgoston, and P. A. Yecko, "An experimental test bed for multi-robot tracking of manifolds and coherent structures in flows," in *Proc. ASME Dyn. Syst. Control Conf.*, Oct. 2013.
[33] G. S. Sukhatme, A. Dhariwal, B. Zhang, C. Oberg, B. Stauffer, and D. A. Caron, "Design and development of a wireless robotic networked aquatic microbial observing system," *Environ. Eng. Sci.*, vol. 24, no. 2, pp. 205–215, 2007.
[34] R. Smith, J. Das, H. Heidarsson, A. Pereira, F. Arrichiello, I. Cetnic, L. Darjany, M.-E. Garneau, M. Howard, C. Oberg, M. Ragan, E. Seubert, E. Smith, B. Stauffer, A. Schnetzer, G. Toro-Farmer, D. Caron, B. Jones, and G. Sukhatme, "USC CINAPS builds bridges," *IEEE Robot. Autom. Mag.*, vol. 17, no. 1, pp. 20–30, Mar. 2010.

Authors' photographs and biographies not available at the time of publication.